JOURNAL OF SPACECRAFT AND ROCKETS
Vol. 42, No. 3, May–June 2005

Solar Arrays for Direct-Drive Electric Propulsion: Electron Collection at High Voltages

Ioannis G. Mikellides* and Gary A. Jongeward†
Science Applications International Corporation, San Diego, California 92121
T. Schneider‡
NASA Marshall Space Flight Center, Huntsville, Alabama 35812
and
T. Peterson,§ T. W. Kerslake,¶ and D. Snyder**
NASA John H. Glenn Research Center at Lewis Field, Cleveland, Ohio 44135

Solar array technologies that can empower electric thrusters in direct drive mode may provide significant mission benefits by reducing power processing, system complexity, weight, and cost over conventional systems. In direct-drive systems the solar arrays will operate at high voltages and must perform safely in the surrounding plasma environment, with minimal loss of performance due to parasitic current collection. For example, current state-of-the-art Hall effect thrusters in the kilowatt class require applied voltages of 300 V or higher. Results from experiments and modeling of electron current collection at high bias voltages (300–500 V) are presented. The experiments employed two sample solar array coupon technologies. A hollow cathode was used to emulate the induced environment around the solar arrays far from the Hall thruster and in nearby regions populated by charge-exchange plasma (10^{12}–10^{13} m^{-3} and 0.5–1 eV). The measurements show that tens to hundreds of seconds are required before the collected current relaxes to a quasi-steady value. Comparisons with results from numerical calculations suggest that changes of the secondary electron yield properties of the dielectric materials may account for the observed current collection trends.

Nomenclature

A_{th} = effective (sheath) collecting area, m^2
d = coverglass thickness, m
$E_\perp$ = perpendicular component of the electric field, V/m
$E_{//}$ = parallel component of the electric field, V/m
e = electron charge, C
I_{col} = collected electron current, A
J = surface current per unit length, A/m
j = total current density, A/m^2
j_e = emitted electron current density, A/m^2
$j_{\text{e,p}}$ = incident current density of primary electrons, A/m^2
j_{th} = electron thermal current density, A/m^2
k = dielectric constant
m_e = electron mass, kg
n_e = electron particle density, m^{-3}
t_c = dielectric charging time, s
Y = secondary electron yield
ε_e = mean energy of emitted electrons, J
ε_p = energy of primary electrons, J
ε_0 = electric permittivity of free space, F/m
ρ = charge density, C/m^3
$\sigma_{//}$ = parallel electrical conductivity, Ω^{-1}
τ = collision time between electrons and snapped-over surface, s
ϕ = electrostatic potential, V
ϕ_{cg} = electrostatic potential of dielectric (coverglass), V
ϕ_{gap} = electrostatic potential of cell gap, V

Presented as Paper 2003-4725 at the 39th Joint Propulsion Conference, Huntsville, AL, 20–23 July 2003; received 6 October 2003; revision received 16 March 2004; accepted for publication 26 March 2004.

*Senior Staff Scientist, Defense Technology Group, 10260 Campus Point Drive. Member AIAA.
†Division Manager, Defense Technology Group, 10260 Campus Point Drive. Member AIAA.
‡Physicist, Space Environmental Effects Group, ED31.
§Program Manager, Power and Propulsion Office, NASA GRC 500-103, 21000 Brookpark Road.
¶Aerospace Engineer, Power and Propulsion Office, NASA GRC 500-103, 21000 Brookpark Road.
**Electrical Engineer, Photovoltaics and Space Environments Branch, NASA GRC 302-1, 21000 Brookpark Road.

Introduction

ELECTRIC propulsion, with its highly efficient use of propellant, has long been recognized as the technology of choice for a number of space missions. These include long-duration deep space missions, as well as station keeping for geostationary satellites. Since its conception over three decades ago, the Hall thruster's (see Ref. 1) unique combination of high specific impulse and thrust-to-power ratio established it as a favored propulsion system for a variety of such missions. Employment of these thrusters continues to be evaluated, worldwide, for orbit insertion to low Earth orbit (LEO),[2] geosynchronous orbit,[3] and in more ambitious missions for the human exploration and development of space.[4] A promising systems approach that may significantly reduce the cost and weight associated with the employment of these thrusters onboard both deep space and near-Earth spacecraft is the use of direct drive. A joined NASA/U.S. Naval Research Laboratory effort conducted in the late 1990s demonstrated that direct-drive operation with a Hall thruster is indeed a viable option (see Ref. 5).

In a conventional electric propulsion system, power is supplied by low-voltage solar arrays (usually <150 V). The high voltages needed to operate the electric thruster are provided by the (propulsion) power processing unit. If the array could provide the required voltage directly, the power processing electronics and heat rejection system would be smaller and lighter. The reductions would translate directly into cost savings and/or allow for additional payload.

This paper and the companion paper by Schneider et al.[6] document results from tests and from modeling that have been performed for the ultimate purpose of defining an envelope of safe operation of the direct-drive Hall thrusters in the presence of high-voltage solar arrays. The results, however, apply not only to direct-drive systems but to other high-voltage space applications as well, such as megawatt-level electric propulsion power systems[7] and the space solar power satellite technology.[8] For the direct-drive Hall-effect thruster (D2HET) system, the assessments have been carried out largely through ground experiments. Wherever possible the experiments have also been supported by modeling and simulation. The plasma environment under which the sample solar array coupons have been tested represents typical conditions under which the flight D2HET solar arrays would be exposed during thruster operation. Such conditions were defined by three-dimensional modeling and simulation calculations.[9] The calculations assumed a representative 2×2 matrix of thrusters and mission scenarios, specifically the 4-kW class Busek–Primex thruster and the 1.4-kW stationary plasma thruster onboard the Deep Space 1 and EXPRESS spacecraft. A system study has also been conducted to quantify the potential savings of a direct-drive system over conventional technologies and to identify trends that may offer additional benefits at power levels and/or mission scenarios other than the representative 2×2 matrix considered in the D2HET program.[10,11]

The high-voltage tests have been driven mainly by two potentially hazardous plasma interactions: leakage (or parasitic) currents and arcing. The first will reduce solar array performance, which can in turn affect the overall spacecraft design if the collected electron current is a significant fraction (more than a few percent) of the current generated by the array. At the higher operating voltages, enhanced parasitic currents can easily occur when dielectric surfaces "snap over." Commonly termed snapover, the phenomenon is the shift in the mechanism by which a dielectric achieves current balance, from repelling most of the incoming electrons to emitting secondary electrons. These secondary electrons are emitted as a result of primary electron bombardment of the dielectric surface and get collected by the nearby conductor (which is usually positively biased), leading to a sudden increase in both current collection and dielectric potential.

Arcing, which is most prominent when the conducting surfaces such as exposed interconnects or semiconductor edges are at a negative potential with respect to nearby insulating surfaces, for example, when the HET is not operating, can lead to permanent electrical shorts. Most efforts to investigate the causes of these and other array failures have concentrated at voltages less than 300 V (Refs. 12–15).

This paper presents electron collection measurements and modeling of two candidate solar array technologies: 1) a design based on the International Space Station (ISS) solar array technology and 2) a design that is representative of the newer, more efficient advanced triple-junction technologies that utilize indium/gallium/arsenide/germanium semiconducting materials. For brevity, in this paper, we refer to the sample coupons used for the tests as the coupon 1 for the ISS design and coupon 2 for the second design. Assessments of arcing initiation and damage from sustained discharges are described by Schneider et al.[6]

Solar Array Designs

A variety of solar array concepts have been considered, some of which employ interconnect shielding from the plasma, array string layout patterns, spacing and grouting, isolation diodes, substrate structural makeup, and multilayer insulation. The two main technologies that have been tested are described next.

Coupon 1

Several of the technology characteristics mentioned apply to the ISS solar array. Despite its lower efficiency compared to newer, multijunction designs such as that represented by coupon 2, the ISS design was chosen as a D2HET candidate due to its relative maturity and demonstrated operation in space. Moreover, both on-orbit observations and modeling of ISS cells operating at voltages less than 150 V suggested that the gap geometry shields the exposed semiconductor edges from the plasma and may, therefore, offer a natural isolation from the environment. No such shielding, however, has been confirmed at the higher voltages (>300 V) of interest here, where snapover of insulating surfaces is expected to, in fact, suppress any electric potential barriers and enhance electron current collection.

Coupon 1 is shown in Fig. 1. The 15-cell coupon was part of an 80-cell panel (16×5 cells) fabricated for the International Space Station Phase 01 Mir Cooperative Solar Array Program. The solar cell panel coupon design, materials, and fabrication techniques are identical to those used in the ISS photovoltaic power module (PPM) with two exceptions: 1) The solar cell submodule is 2×5 cells

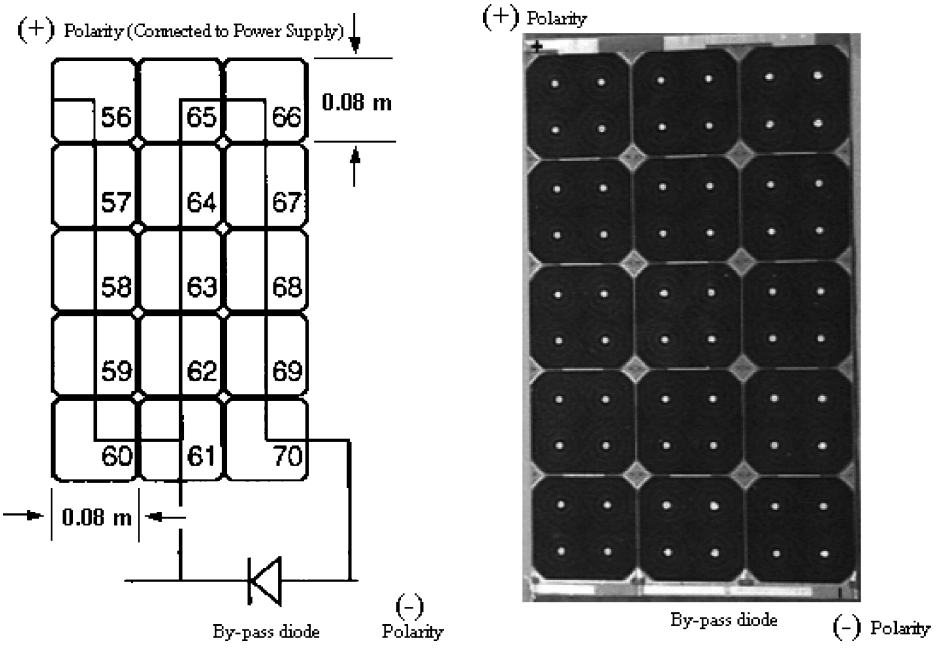

Fig. 1 Coupon 1 sample used for the electron current collection tests.

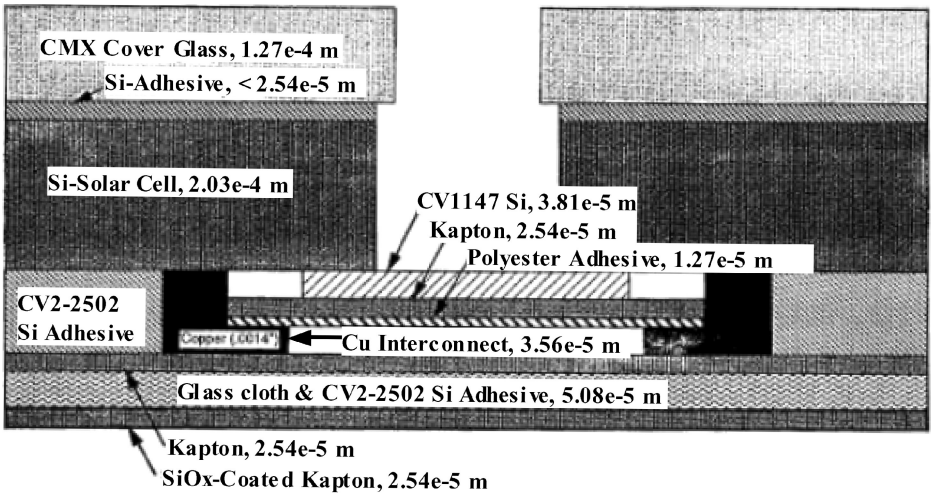

Fig. 2 Cutaway view of adjacent solar cells in coupon 1 with approximately 0.05-mm cover glass overhang.

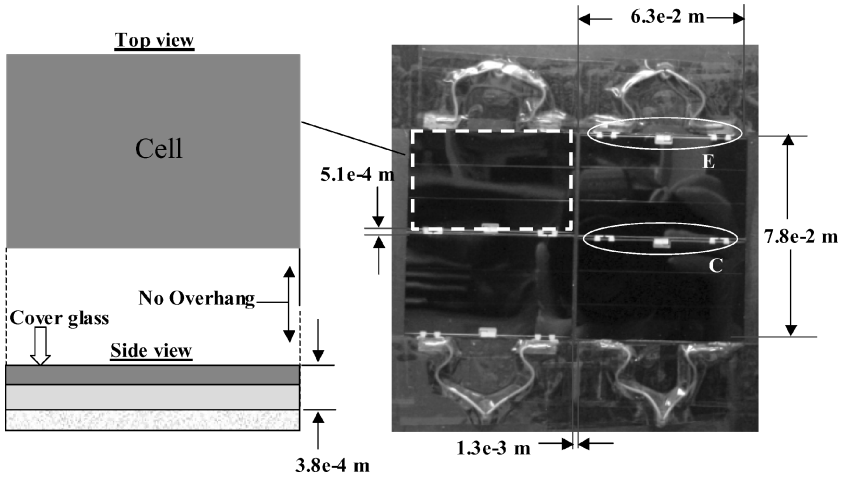

Fig. 3 Coupon 2 sample used in the electron current collection tests.

(instead of 2×4) and 2) a pair of small diameter "button holes" is introduced in the substrate between solar cells. The latter feature was used to attach the solar cell panels to Russian-built solar array frames. The coupon positive polarity tab (shown to come off cell 56 in Fig. 1a) is connected to the cell p contacts, whereas the negative polarity tab (off cell 70 in Fig. 1a) is connected to the cell n contacts. A bypass diode is connected between cells 70 and 61. A cutaway view of two adjacent cells is shown in Fig. 2.

Coupon 2

The second design is shown in Fig. 3. It comprises two solar power modules (SPM), each containing two solar cells as shown on the right of Fig. 3. The solar cell is made of gallium indium phosphide/gallium arsenide (GaInP/GaAs) on a germanium (Ge) substrate (active junction). This technology was chosen primarily due to its higher efficiency (GaInP/GaAs/Ge cells have reportedly demonstrated >30% efficiency under concentrated light.[16]) In contrast to coupon 1, coupon 2 utilizes conventional interconnects that may lead to greater electron collection. The exposed interconnects also increase the possibility of arcing. However, an SPM covers multiple cells with a coverglass. In the sample coupon, the coverglass covers two cells (in the vertical direction as shown in Fig. 3) thus, isolating interior interconnects from the plasma almost completely (circled and labeled C in Fig. 3). Those interconnects that lie around edges, however, are partially exposed. To emulate this arrangement in the laboratory, Kapton® tape was placed on top of part of the edge interconnects (circled, labeled E in Fig. 3) leaving approximately one-half of their area exposed. Also in contrast to coupon 1, the coverglass does not extend over the solar cell in the direction of the adjacent SPM, thus, leaving no overhang. The coverglass material is made of silica microsheet and is bonded to the cell with silicon adhesive. The substrate materials consist of Kapton tape laid on top of graphite layer.

Facilities

Two vacuum chambers at NASA Marshall Space Flight Center were utilized for the tests. The first chamber with coupon 1 sample is shown in Fig. 4a. The second chamber with the mounted coupon 2 is shown in Fig. 4b. Both arrays were electrically isolated from their supporting structure during the tests. The first chamber is approximately 1 m in diameter and 2 m long. Two liquid nitrogen trapped diffusion pumps provide the vacuum. A hollow cathode with an annular keeper electrode has been used to simulate the HET plasma conditions in the vacuum chamber. The source was constructed was operated with argon. The second chamber is of similar dimensions and capabilities and was used later in the D2HET program for both electron collection and arcing tests.

Plasma particle densities in the range from high (10^{11}) to low (10^{13} m^{-3}) and electron temperatures on the order of 0.5–1 eV were produced in the vacuum chambers. The plasma conditions were chosen to represent the relevant plasma environment around the solar arrays during operation of the thrusters. The plasma environment was estimated by performing three-dimensional calculations with the electric propulsion interactions code (EPIC).[17]

With the plasma source off, the chamber pressure was about 5×10^{-7} torr. During the operation of the source, the background pressure was ranged from high to low (10^{-5}–10^{-4} torr). Various diagnostics were used to determine the plasma conditions around

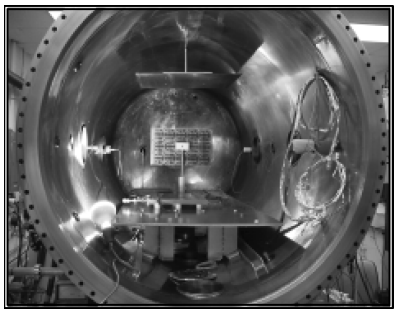

a)

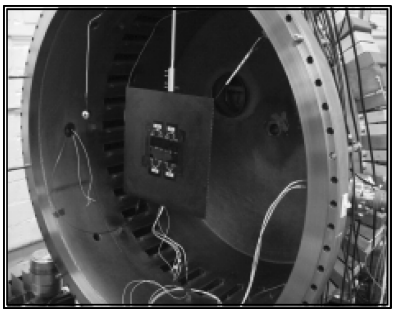

b)

Fig. 4 Vacuum chambers employed for the tests: a) coupon 1 and b) coupon 2.

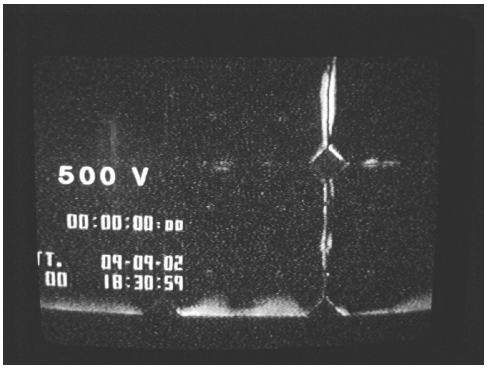

Fig. 5 Photograph of coupon 1 immersed in a plasma at a bias voltage of 500 V.

the array segments, which are described in greater detail in Refs. 6 and 9.

Results from Experiments and Modeling

Experiments

Electron collection measurements during early tests, with one of two samples of the 3×5 coupon 1, were performed by positively biasing the coupon with respect to ground. The two sample coupons were cut out of the same 80-cell PPM. Current collection measurements were obtained using the first of the two coupons (coupon 1-A throughout this paper) at 100-ms increments. The bias voltage sweeps ranged from 0 to 500 V (Ref. 9). Figure 5 shows a closeup photograph (showing approximately 3×2 cells) of coupon 1-A during electron collection at a bias voltage of 500 V. The 100-ms time increment was deemed sufficiently large to allow for the relaxation of transient effects associated with dielectric charging. Specifically, in the ideal case of an insulating planar surface element of thickness d, the charging time t_c to reach current balance, that is, the sum of all currents equal zero at the surface, at a potential ϕ_{cg} would be determined by

$$\int_0^{t_c} \mathrm{d}t = \frac{k\varepsilon_0}{\mathrm{d}} \int_0^{\phi_{cg}} \frac{\mathrm{d}\phi}{j(\phi)} \tag{1}$$

with j being the total current density at the surface. For the 5-mil-thick cover slide of the coupon in Fig. 2, the maximum charging t_c that could be attained would be if the mean current density to the surface during charging was taken to be the thermal current density ($j = j_{th} = 200\ \mathrm{mA/m^2}$), and ϕ_{cg} was taken to be the cell bias voltage, for example, 500 V. Under these conditions, t_c would be 0.6 ms (using a dielectric constant value for the cover glass to be $k = 3.5$). In reality, when the dielectric is snapped over, it is expected that the mean (net) current density to the surface would be higher than the thermal value and the charging voltage would be lower than the cell bias voltage. Thus, the charging time would be much less than 0.6 ms. Despite such short relaxation times, the current-voltage (I-V) measurements exhibited large fluctuations, lacking reproducibility under similar plasma conditions.

To eliminate transient effects, the coupon was allowed to collect electrons for times greater than 300 s at each (fixed) bias voltage. Figures 6 and 7 show representative signals collected during the period 5–11 September 2002 by using the original coupon 1-A at 300 and 500 V, respectively. The identical sample, coupon 1-B, exhibited similar transient behavior. Figures 8 and 9 show electron current collected after exposure to the plasma for 300 s, for coupons 1-A and 1-B, respectively. A notable distinction between the two coupons is that coupon 1-A surfaces were exposed to the plasma

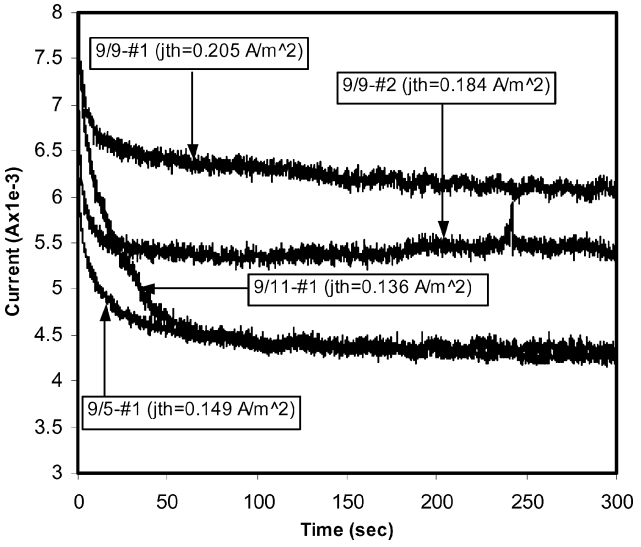

Fig. 6 Representative transient data for coupon 1-A biased to 300 V: $n_e = 0.5$–$1.\ 4e13\ \mathrm{m}^{-3}$, $T_e = 0.4$–0.6 eV, and $p = 6$–$9e{-}5$ torr.

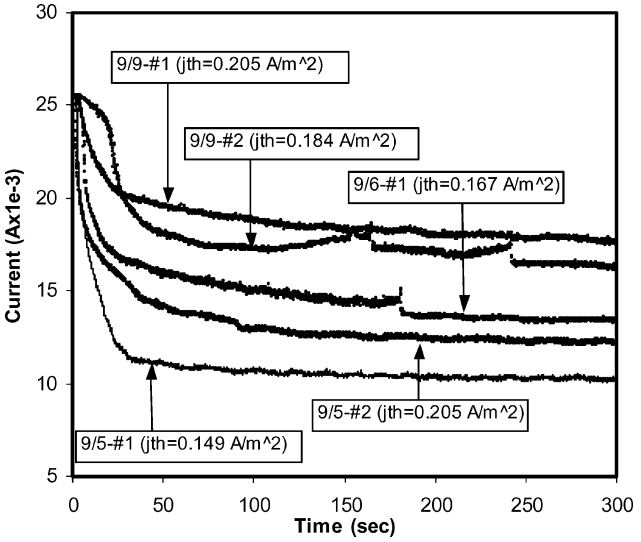

Fig. 7 Representative transient data for coupon 1-A biased to 500 V: $n_e = 0.5$–$1.\ 4e13\ \mathrm{m}^{-3}$, $T_e = 0.4$–0.6 eV, and $p = 6$–$9e{-}5$ torr.

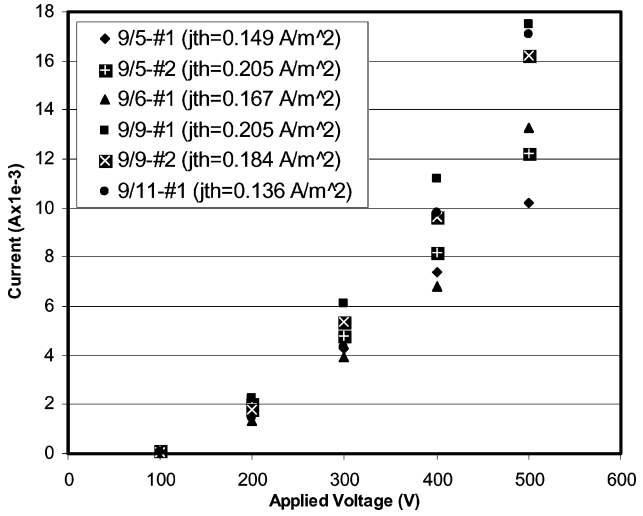

Fig. 8 Electron current collected by coupon 1-A after 300 s, on various days during the September 2002 tests.

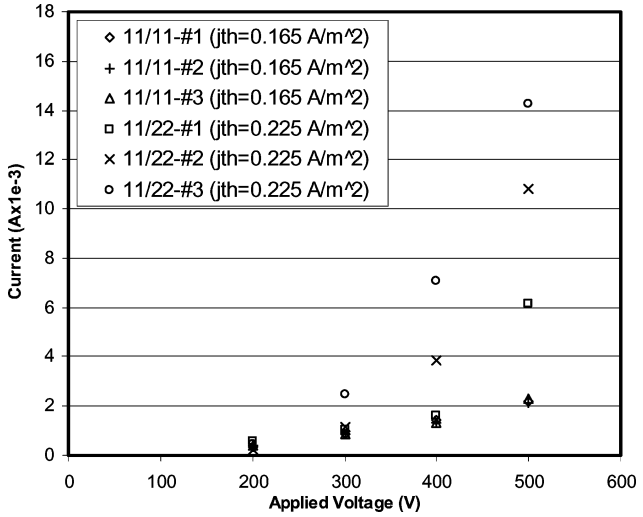

Fig. 9 Electron current collected by coupon 1-B after 300 s, on various days during the November 2002 tests.

for much longer time because the sample had also been used during the earlier tests. More specifically, Fig. 9 shows the very first data acquired from the tests of coupon 1-B sample; Fig. 8 shows data toward the end of testing of coupon 1-A. By then, coupon 1-A had accumulated hundreds of hours of exposure to the plasma.

The data reveal two main trends for coupon 1: 1) Relaxation time is in the order of tens to hundreds of seconds. 2) The variability (standard deviation divided by the mean value) of collected current after exposure to the plasma for 300 s generally increases with bias voltage, ranging 13–27% for coupon 1-A and 26–71% for coupon 1-B. Coupon 1-B also collected higher currents the longer the coupon was tested (Fig. 9). Similarly to coupon 1, coupon 2 also exhibited transient behavior and large variability at each bias voltage for most cases (Fig. 10). As shown in Fig. 11, however, many cases (at 500 V) did not exhibit large variations from the steady-state value. By comparison with the 400-V case, it is observed that those cases at 500 V that exhibited almost steady-state behavior were sustained at values less than 0.4 mA. This value is lower than any of the values recorded in the 400-V case. For example, the steady-state current collected during the 18 November test 1 and 21 November test 1 tests are approximately 0.3 mA, which is comparable to the highest current collected in the 300-V case (Fig. 12). The signals corresponding to 18 November test 3 and 21 November test 3 shown in Fig. 11 are at ~0.16 mA, which is comparable to the highest current values observed in the 200-V case (Fig. 12). Thus, it is possible that for the 500-V signals in question only portions of the exposed

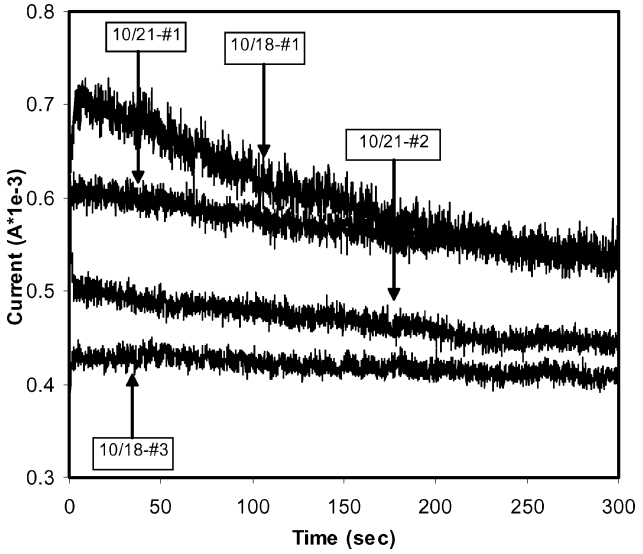

Fig. 10 Representative current signals for coupon 2 biased to 400 V, all signals normalized to $j_{th} = 200$ mA/m^2. Actual values of j_{th} are $j_{th} = 227.4$ mA/m^2, 18 November and, $j_{th} = 270.8$ mA/m^2 21 November (range of conditions: $n_e = 1$–$1.6e13$ m^{-3}, $T_e = 0.4$–0.6 eV, and $p = 6$–$9e{-}5$ torr).

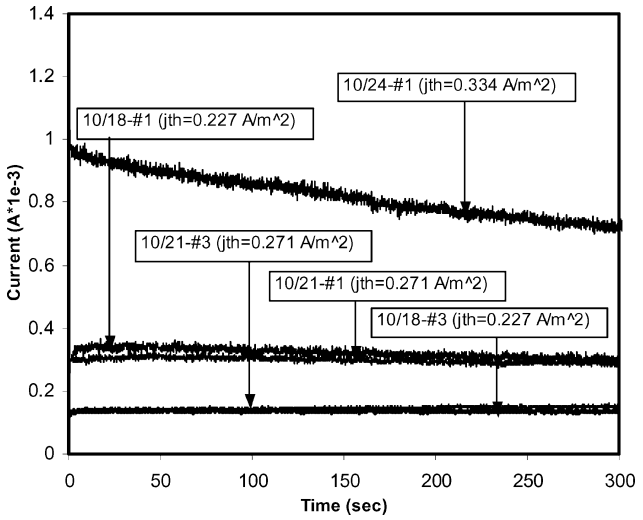

Fig. 11 Representative current signals for coupon 2 biased to 500 V: $n_e = 1$–$1.6e13$ m^{-3}, $T_e = 0.4$–0.6 eV, and $p = 6$–$9e{-}5$ torr.

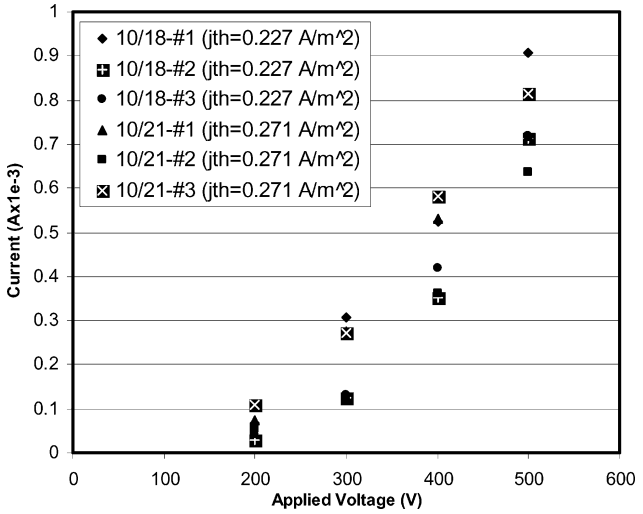

Fig. 12 Electron current collected by coupon 2 after 300 s, on various days during October 2002 tests.

semiconductors were collecting electrons. These measurements (18 November test 1, 21 November test 1, 18 November test 3, and 21 November test 3) are, therefore, not used to support any of the conclusions presented in this effort. Moreover, in contrast to coupon 1, the variability generally decreased with increasing bias voltage, from 43% (at 300 V) to 18% (at 500 V).

Table 1 lists average values of electron current collection after 300 s, scaled to nominal plasma density of 10^{13} m^{-3} and electron temperature of 0.55 eV. The scaling in Table 1 is based on the thermal current density and is only an assumption. In reality, current collection depends on both the plasma conditions and the sheath around the cell gaps. However, at the high bias voltages studied here, the insulators have snapped over, the sheath is very large compared to the cell gaps, and the plasma conditions do not very greatly for each case. Under these conditions, it is assumed that the plasma conditions perturb the sheath only slightly. Thus, the collected current is assumed to scale with the thermal current density j_{th}. The scaled values were used to determine the variability of the measurements at each bias voltage. Finally, note that the waiting time between current collection measurements in each day of testing did not alter the transient trends presented herein. The waiting time was varied from almost no time to more than 300 s. Between days, for many of the cases presented here the coupons were exposed to air.

In the absence of charging effects, other mechanisms that may possibly lead to the prolonged times observed during current collection are considered. For example, numerous studies on the adverse effects of electron clouds on high-energy particle accelerator facilities involved measurements of the change in secondary electron yield (SEY) properties with charged-particle dose (in units of charge per unit area) for various metals.[18–20] These efforts were primarily motivated by the need to reduce the electron cloud generated by secondary electron emission of metal surfaces. One proposed way to reduce this effect is to condition the emitting surface by exposing it to electron doses that are sufficiently high to reduce permanently its SEY characteristics. It was found that under specific conditioning the SEY could indeed be permanently altered; if the conditioning was insufficient the change would not be permanent. The results from one such study[18] on copper are shown in Fig. 13.

Table 1 Average electron current collected[a] by coupons 1 and 2 (after 300 s) at $j_{th} = 200$ mA/m^2

Applied voltage, V	Coupon 1-A average I, mA	Coupon 1-B average I, mA	Coupon 2 average I, mA	Coupon 2 ($\times A_1/A_2$) average I, mA
200	2.038	0.407	0.055	0.233
300	5.538	1.201	0.180	0.776
400	10.31	2.687	0.405	1.745
500	16.88	5.974	0.661	2.875

[a]Coupon collecting areas: $A_1 \approx 9.75e$–4 m^2 (coupon 1) and $A_2 \approx 2.07e$–4 m^2 (coupon 2).

Modeling

Preliminary two-dimensional simulations of coupon 1 current collection tests were conducted by using the finite element electrostatic code Gilbert, in conjunction with analytical modeling. Gilbert solves Poisson's equation for the electrostatic potential ϕ, in two-dimensional planar geometry:

$$\nabla^2\phi = -\rho/\varepsilon_0 \tag{2}$$

using a nonlinear profile for the charge density ρ appropriate for most LEO plasma environments.[21] The calculations showed that in the absence of snapover an electron potential barrier would form approximately 100 mil from the cell gap. Barriers form because the cover glass charges to a few volts negative as ions and electrons achieve current balance at the insulating surface. At low voltages (<150 V), two-dimensional numerical calculations suggest that snapover does not occur. At such low voltages, the use of argon (the gas used during the tests) rather than xenon (commonly the propellant of choice for Hall thrusters) can lead to different current collection characteristics. Specifically, because the xenon ion is heavier, the cover glass would charge to a more negative potential value than it would in the presence of argon ions. In steady state the cover glass potential can be estimated to be $-5.6T_e$ V for Ar and $-6.2T_e$ V for Xe (Ref. 9). Consequently, when two-dimensional orbit-limited current collection that includes the effects of potential barriers is assumed,[9] and with all other conditions (such as the gap potential and electron temperature) remaining unchanged, current collection could be reduced by about a factor of two in a xenon plasma. Preliminary two-dimensional calculations suggest that, in the absence of snapover, orbit-limited current collection at the higher voltages of interest in D2HET (>250 V) greatly underestimates the measurements.[9]

Additional calculations have, therefore, been performed that allowed surfaces to snap over. Gilbert incorporates a model for snapover electric field boundary conditions from Ref. 21 and is summarized here for completeness. It is assumed that the snapped-over surface has an electron-attracting component of the electric field $E_\perp$ and emits a low-energy electron current density j_e. These electrons "hop" along the surface in parabolic orbits with characteristic time between collisions (with the surface) that is given by

$$\tau = 2\sqrt{2m_e\langle\varepsilon_e\rangle/(eE_\perp)^2} \tag{3}$$

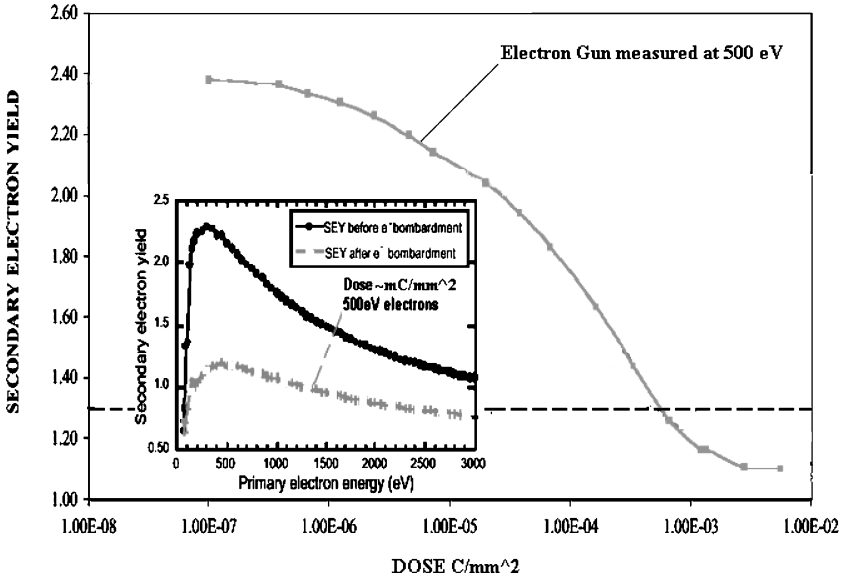

Fig. 13 Variation of SEY properties with electron dose for copper (from Refs. 18–20).

The mean emitted-electron energy is $\langle \varepsilon_e \rangle$ and is taken to be 1–2 eV (where an electron volt is equal to 1.602e-19 J). The layer of electrons created along the surface will be accelerated by any parallel electric field $E_{//}$, leading to surface current per unit length J (in amperes per meter) given by

$$J = j_e(\tau^2/2)(eE_{//}/m_e) = \sigma_{//}E_{//} \tag{4}$$

where $\sigma_{//}$ is the parallel electrical conductivity (in mho),

$$\sigma_{//} = 4j_e\left(\langle \varepsilon_e \rangle / eE_\perp^2\right) \tag{5}$$

When it is assumed that the emitted current is proportional to the incident current density of primary electrons $j_{e,p}$ according to

$$j_e = Y(\varepsilon_p)j_{e,p} \tag{6}$$

with $Y(\varepsilon_p)$ being the SEY as a function of primary-electron energy ε_p, then charge conservation $j_{e,p} = \nabla \cdot J$ leads to

$$j_{e,p} = (4/e)Y(\varepsilon_p)j_{e,p}\langle \varepsilon_e \rangle\left(\nabla \cdot E_{//} / E_\perp^2\right)$$

$$\Rightarrow E_\perp = \sqrt{(4/e)Y(\varepsilon_p)\langle \varepsilon_e \rangle \nabla \cdot E_{//}} \tag{7}$$

Equation (7) is the desired electric field boundary condition. The value of ε_p was computed by using the local value of the surface potential and was determined by iteration with the overall solution to Eq. (2).

Two cases of SEY $Y(\varepsilon_p)$ as a function of primary electron energy that have been used in the snapover calculations are shown in Fig. 14. The thick curve shows the form used for SiO_2 when it is assumed that no conditioning of the insulating surfaces due to electron bombardment has taken place.[22] The thin curve is an assumed form used to estimate the SEY reduction by the electron dose. To the best of our knowledge, no data exist to date on the variation of silica-based cover glass and substrate material SEY with electron dose. In the absence of such data and in view of the similarity of the SEY forms between copper (Fig. 13, lower left corner) and SiO_2 (Fig. 14, thick curve) at zero dose, one case of the SEY reduction was estimated by assuming that the primary electron current density to the insulators is equal to the thermal current density j_{th}. Thus, the insulators received a dose approximately equal to

$$\text{dose} \approx t j_{th} = (300\text{ s})200\,\text{mA/m}^2 = 60\,\mu\text{C/mm}^2 \tag{8}$$

At this dose, the variation of the maximum SEY for the case of the electron gun at 500 eV in Fig. 13 suggests a maximum value of 1.85. We use this value and the universal functional form of the SEY[22] (without changing the energy at peak SEY = 400 eV) to compute the dose-affected SEY. Higher flux values, which would be more appropriate for the substrate insulators, have been estimated by using the collected current divided by the collecting area. At

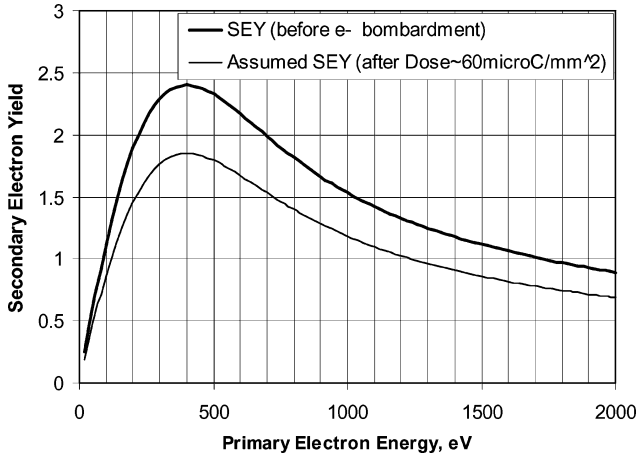

Fig. 14 Secondary electron yield curves used for the calculations involving snapover of insulators.

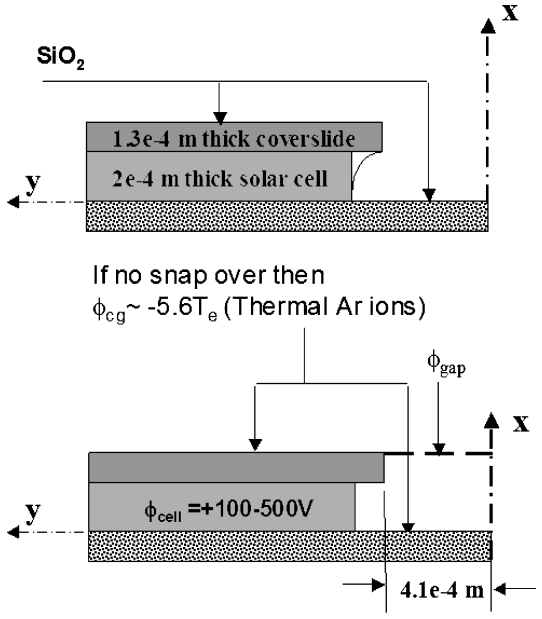

Fig. 15 Arrangement used for the two-dimensional numerical calculations.

500 V, for example, with the data from the coupon 1-A tests, the flux would be in the order of a few to more than 10 A/m^2, which would mean a dose greater than 1 mC/mm^2. At these higher values, the peak SEY for copper is observed to change only slightly with increasing dose. A value of 1.2 was chosen as the maximum yield to represent this region of SEY as a function of dose. We reiterate here that the second-long timescales observed in the experiments are much longer than the characteristic dielectric charging times (<1 ms, as already shown). Therefore, in the present calculations, the net current to the insulator is assumed to be zero. The current density used in the estimation of the dose received by the insulator is that of the primary electrons.

The two-dimensional planar geometry used for the simulations is summarized in Fig. 15. The electric potential contours close to the solar cell gap have been computed by using Gilbert for a cell bias of 300 V and are shown in Fig. 16. Note that at these higher voltages, when the surfaces have snapped over, the influence of potential barriers on the solution is negligible (less than 1e-2 V magnitude of barrier potential) because the insulator surfaces that are at a negative potential are far from the cell gaps. Thus, the smaller (in magnitude) cover glass potential associated with argon ions (used during the tests) is not expected to introduce major differences in the electron current collection by comparison to xenon, the propellant of choice for Hall thrusters. Other disparities between the two gases, such as the effects of ionization on the sheath in the presence of snapped-over surfaces, would be less easy to predict and would, therefore, require more analysis and testing.

The result shown in Fig. 16 is for a peak SEY of 2.4. To compute the collected current we assume that the cells collect all thermal electrons. At the nominal conditions assumed for the calculations, $n_e = 10^{13}$ m^{-3} and $T_e = 0.55$ eV ($\Rightarrow$ $j_{th} = 200$ mA/m^2); this corresponds to electron thermal energy per unit charge of $V_{th} = \frac{1}{2}(m_e/e)[8k_BTe/\pi m_e] = 0.7$ V. The location of the 0.7-V contour was determined by Gilbert and was then used to determine the collecting area A_{th}. The electron current collected I_{col} is then estimated by

$$I_{col} \approx j_{th}A_{th} \tag{9}$$

Although a more accurate calculation would incorporate electron tracking to the collecting surface (e.g., that of Mandell and Katz[23]) estimation (9) can still provide a quantitative trend that may be compared with the data to assess the effects of SEY properties on current collection. Table 2 shows the results of several calculations using different SEY forms and the data from the coupons 1-A and

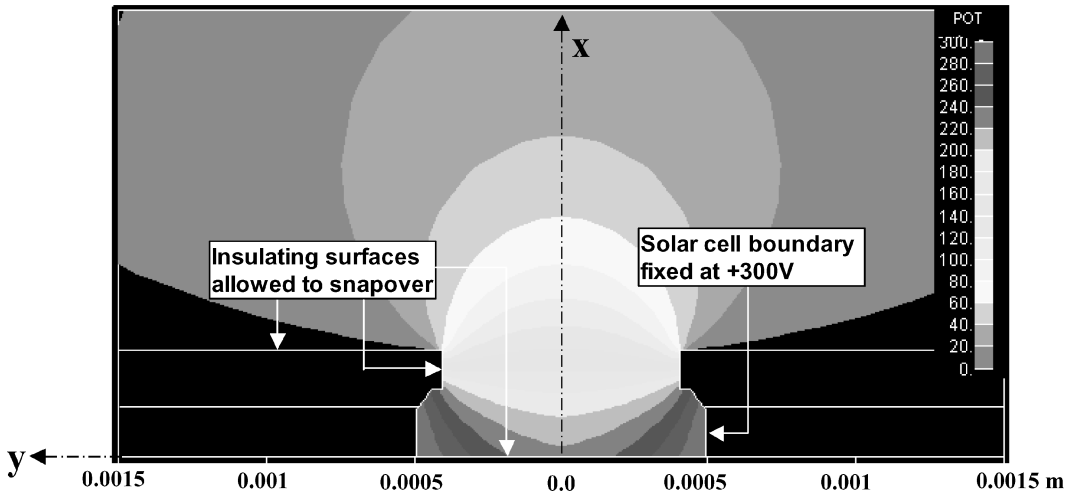

Fig. 16 Electric potential contours computed for the case of a solar cell bias of +300 V; cell geometry emulates that of coupon 1 (see Fig. 2).

Table 2 Comparisons between current collection[a] data for the coupon 1 samples and calculations using different secondary electron yields

	Applied voltage, V			
Case	200	300	400	500
Coupon 1-A, mA				
Maximum	2.19	6.36	14.7	25.1
Minimum	1.92	4.52	7.85	10.8
Coupon 1-B, mA				
Maximum	0.46	2.20	6.28	12.7
Minimum	0.21	1.02	1.63	2.6
Computed values, mA				
$Y_{max} = 2.4$	7.34	11.7	G	G
$Y_{max} = 1.85$	1.29	11.9	14.7	G
$Y_{max} = 1.2$	B	B	8.08	16.9

[a]Collected current data scaled to $j_{th} = 200$ mA/m^2.

1-B samples. Grid size limitations did not allow calculations for a few cases, which are indicated by G in the table. B indicates cases for which potential barriers could no longer be ignored. For these cases, the computed values would predict much less current than what has been measured and have, therefore, not been computed numerically. The peak SEY values for the calculations were selected to represent the following cases: 1) no dose effects ($Y_{max} = 2.4$), 2) dose effects assuming only thermal electron flux bombarding the insulators ($Y_{max} = 1.85$) and the maximum dose effect, and 3) assuming an electron flux based on the collected current at 500 V ($Y_{max} = 1.2$). The comparisons of Table 2 suggest that changes in the SEY properties of the dielectric may indeed account for the observed variation of electron collection with bias voltage. However, both the lack of SEY measurements for the dielectric material on the coupon 1 sample and the significant variability in current collection observed during the tests do not allow for a more conclusive assessment based on the comparisons made between theory and experiment.

Summary

Two solar array technologies have been tested for electron current collection at voltages higher than 200 V, as part of an effort to assess solar array technologies for application to direct-drive Hall effect electric propulsion systems. The first technology sample was a coupon containing (3×5) cells that are identical to the ISS backside connection design. The second coupon was a newer SPM design employing (conventional) interconnects. The interconnects were partially exposed to the surrounding plasma during the tests. Both coupons exhibited transient variations in current collection with characteristic times that greatly exceeded the dielectric charging time. After many hours of exposure to the plasma, the first of two 3×5 coupons (coupon 1-A) cut from the same 80-cell PPM, collected 2–5 times more current than its counterpart (coupon 1-B) did when first tested. Coupon 1-B, however, also exhibited noticeable increase in current collected with increasing exposure to the plasma. Thus, the large differences in the magnitude of collected current (in steady state) between the two identical coupons 1-A and B may be attributed to 1) possibly tainted surfaces of coupon 1-B, which did not have the chance of being cleaned-off by the plasma (contrary to coupon 1-A which was exposed to the plasma for many more hours), and/or 2) permanent property changes or hardening of the collecting surfaces and surrounding insulators of coupon 1-A after many hours of testing.

Coupon 2 also displayed transient collection for most of the measurements. For a few cases at a bias voltage of 500 V, current collection occurred without much deviation from the steady-state value. A comparison, however, between the current collection measurements at 400 and 500 V suggests that those current signals that exhibited almost steady-state behavior at 500 V were sustained at values of less than 0.4 mA. This is despite the fact that the two cases were conducted during the same days under similar plasma environments. These current values are less than any of the values recorded in the 400-V case. Thus, in those 500-V cases for which no major transient behavior was observed, it is possible that only portions of the exposed semi-conductors were collecting electrons. The reason(s) that may have led to such behavior is unknown. Finally, all coupons showed large variability from the steady-state mean value.

Modeling of current collection for coupon 1 suggests that changes in the SEY properties of the dielectric materials may be playing a significant role in the amount of current collected at high electron densities and high bias voltages. Calculations in the absence of snapover boundary conditions would greatly underestimate the measured values of collected current. The calculations presented here, which allowed for snapover, overestimate the data if no change in the SEY is assumed. Better agreement is achieved after assuming that the insulator SEY properties had been reduced due to incident electron dose. The reduced SEY curve was deduced from existing data on copper. Although the dose-independent SEY curves for copper and SiO_2 (the assumed material for the present calculations) are similar, the sensitivity of current collection to SEY properties emphasizes the importance of such measurements on solar array insulator materials. Until such data become readily available, the predictive capability of theoretical models for high-voltage arrays (>300 V), such as the one presented in this effort, will be weak.

Acknowledgments

This work was conducted under NASA Contract NAS3-01100. The authors thank E. Watts for valuable assistance in gathering the data. We also acknowledge the contributions of the remaining D2HET team members, A. Hoskins, D. Ferguson, M. Hovater, M. R. Carruth, and D. King.

References

[1]Morozov, A. I., Esipchuk, Y. V., Tilinin, G. N., Trofimov, A. V., Sharov, Y. A., and Shchepkin, G. Y., "Plasma Acceleration with Closed Electron Drift and Extended Acceleration Zone," *Soviet Physics—Technical Physics*, Vol. 17, No. 38, 1972, pp. 32–37.

[2]Oleson, S. R., "Electric Propulsion for Low Earth Orbit Communications Satellites," International Electric Propulsion Conf., IEPC Paper 97-102, Aug. 1997.

[3]Oleson, S. R., and Myers, R. M., "Advanced Propulsion for Geostationary Orbit Insertion and North–South Station Keeping," *Journal of Spacecraft and Rockets*, Vol. 34, No. 1, 1997, pp. 22–28.

[4]Oleson, S. R., and Sankovic, J. M., "Advanced Hall Electric Propulsion for Future In-Space Transportation," NASA TM-2001-210676, April 2001.

[5]Hamley, J. A., Sankovic, J. M., Lynn, P., O'Neill, M. J., and Oleson, S. R., "Hall Thruster Direct Drive Demonstration," AIAA Paper 97-2787, July 1997.

[6]Schneider, T. A., Mikellides, I. G., Jongeward, G. A., Peterson, T., Kerslake, T. W., Snyder, D., and Ferguson, D., "Solar Arrays for Direct-Drive Electric Propulsion: Arcing at High Voltages," *Journal of Spacecraft and Rockets*, Vol. 42, No. 3, 2005, pp. 543–549.

[7]Kerslake, T. W., and Gefert, L. P., "Solar Power System Analyses for Electric Propulsion Missions," NASA TM-1999-209289, July 1999.

[8]Dudenhoefer, J. E., and George, P. J., "Space Solar Satellite Technology Development at the Glenn Research Center—An Overview," NASA TM-2000-210210, July 2000.

[9]Jongeward, G. A., Mikellides, I. G., Peterson, T., Kerslake, T. W., Ferguson, D., Snyder, D., Carruth, M. R., Schneider, T., Hovater, M., Hoskins, A., King, D. Q., and Ralph, E. L., "Development of a Direct Drive Hall Effect Thruster System," Society of Automotive Engineers Power Systems Conf., SAE Paper 02PSC-77, Oct. 2002.

[10]Hoskins, A., Homiak, D., Cassady, R., Kerslake, T., Peterson, T., and Ferguson, D., "Direct Drive Hall Thruster System Development," AIAA Paper 2003-4726, July 2003.

[11]Kerslake, T. W., "Effect of Voltage Level on Power System Design for Solar Electric Propulsion Missions," International Solar Energy Conf., Paper ISEC2003-44008, March 2003.

[12]Katz, I., Davis, V. A., and Snyder, D. B., "Mechanism For Spacecraft Charging Initiated Destruction of Solar Arrays in GEO," AIAA Paper 98-1002, Jan. 1998.

[13]Jongeward, G. A., Katz, I., Mandell, M. J., and Parks, D. E., "The Role of Unneutralized Surface Ions In Negative Potential Arcing," *IEEE Transactions on Nuclear Science*, Vol. 32, Dec. 1985, pp. 4087–4091.

[14]Cho, M., Ramasamy, R., Matsumoto, T., Toyoda, K., Nozaki, Y., and Takahashi, M., "Laboratory Tests on 110-Volt Solar Arrays in Simulated Geosynchronous Orbit Environment," *Journal of Spacecraft and Rockets*, Vol. 40, No. 2, 2003, pp. 211–229.

[15]Vayner, B., Galofaro, J., Ferguson, D., and Degroot, W., "Electrostatic Discharge Inception on a High-Voltage Solar Array," AIAA Paper 2002-0631, Jan. 2002.

[16]Green, M. A., Emery, K., King, D. L., Igari, S., and Warta, W., "Solar Cell Efficiency Tables (Version 17)," *Progress in Photovoltaics*, Vol. 9, Jan. 2001, pp. 49–56.

[17]Mikellides, I. G., Mandell, M. J., Kuharski, R. A., Davis, D. A., Gardner, B. M., and Minor, J., "The Electric Propulsion Interactions Code (EPIC): A Member of the NASA Space Environment and Effects Program (SEE) Toolset," AIAA Paper 2003-4871, July 2003.

[18]Baglin, V., Collins, I. R., Henrist, B., Hilleret, N., and Vorlaufer, G., "A Summary of Main Experimental Results Concerning the Secondary Electron Emission of Copper," French European Council for Nuclear Research, Rept. CERN-LHC-Project-Report-472, Geneva, June 2002.

[19]Kirby, R. E., and King, F., "Secondary Electron Emission Yields From PEP-II Accelerator Materials," Stanford Linear Accelerator Center Rept. SLAC-PUB-8212, Stanford, CA, Oct. 2000.

[20]Baglin, V., Bojko, J., Gröbner, O., Henrist, B., Hilleret, N., Scheuerlein, C., and Taborelli, M., "The Secondary Electron Yield of Technical Materials and Its Variation with Surface Treatments," 2000 European Particle Accelerator Conf., CERNLHC Project Rept. 433, Vienna, Sept. 2000.

[21]Mandell, M. J., and Davis, V. A., "User's Guide to NASCAP/LEO," Maxwell Labs., Inc., Rept. SSS-R-85-7300-R2 S-Cubed Div., San Diego, CA, Aug. 1990.

[22]Hastings, D., and Garret, H., *Spacecraft Environment Interactions*, Cambridge Atmospheric and Space Science Series, Cambridge Univ. Press, Cambridge, England, U.K., 1996, p. 150 [eq. (5.5)].

[23]Mandell, M. J., and Katz, I., "High-Voltage Plasma Interactions Calculations Using NASCAP/LEO," AIAA Paper 90-0725, Jan. 1990.

A. Ketsdever
Associate Editor